Applied Radiation and Isotopes 237 (2026) 112839

Contents lists available at ScienceDirect

Applied Radiation and Isotopes

journal homepage: www.elsevier.com/locate/apradiso

# Development of the DUMBO imaging device for beta-emitting radionuclides within the ISOLPHARM collaboration

Davide Serafini [a,b,*], Jessica Carolina Delgado Alvarez [c], Aurora Leso [a,d], Alberto Arzenton [c,e], Devid Maniglio [f], Stefano Corradetti [a], Emilio Mariotti [b,g], Marcello Lunardon [c,e], Piero Giubilato [c,e], Alberto Andrighetto [a]

[a] Legnaro National Laboratories, National Institute for Nuclear Physics, INFN-LNL, Viale dell'Università 2, 35020 Legnaro, Italy
[b] Department of Physical Sciences, Earth and Environment, University of Siena, Via Roma 56, 53100 Siena, Italy
[c] Department of Physics and Astronomy, University of Padova, Via Marzolo 8, 35131 Padova, Italy
[d] Department of Physics and Earth Science, University of Ferrara, Via G. Saragat 1, 44121 Ferrara, Italy
[e] Padova Division, National Institute for Nuclear Physics, Via Marzolo 8, 35131 Padova, Italy
[f] Department of Industrial Engineering, BIOtech Research Center, University of Trento, Via delle Regole 101, 38123 Mattarello, Italy
[g] Pisa Division, National Institute for Nuclear Physics, Largo Bruno Pontecorvo 3, 56127 Pisa, Italy

ARTICLE INFO

*Keywords:*
Ag-111
ISOLPHARM
ALPIDE
Imaging
MAPS

ABSTRACT

Existing $\beta$-imaging devices with real-time image reconstruction typically have a field of view (FOV) of about 0.1 $cm^2$, which is too small for imaging large cell cultures as a whole. To provide a complementary tool in radiopharmaceutical research, the Detector Using Maps for Beta-rays Observations (DUMBO) $\beta$-imaging device was developed, featuring lower spatial resolution but a larger FOV and non-invasive imaging capability. The prototype presented in this work consists of two ALICE PIxel DEtector (ALPIDE) chips, providing a total sensitive area of 3 cm × 3 cm. The sample can be positioned with three degrees of freedom, two of which are motorized using commercial stepper actuators. The performance was evaluated through Geant4 simulations and experimental measurements with the medical radionuclide $^{111}$Ag. Plastic and hydrogel phantoms were imaged to assess the device response to different sample types. The circular shape of the vials containing aqueous $^{111}$Ag solutions, as well as the structure of the plastic phantoms with 1–3 mm-wide channels, were clearly resolved. The simulated spatial resolution, which depends on the distance between source and detector, could reach values as good as 0.3 mm; however, sample preparation limited the experimentally achieved resolution. DUMBO demonstrated stable operation, straightforward sample handling, and clear detection capability for samples with activities of the order of 100 kBq.

## 1. Introduction

### 1.1. Experiments requiring beta-imaging

Targeted Radionuclide Therapy is an established treatment modality for tumors adopted in clinics (Sgouros et al., 2020). This technique employs a radionuclide-containing drug, the radiopharmaceutical, to deliver lethal damage to cancer cells. It can be applied with different radionuclides suitable for different types of tumors. In particular, $^{111}$Ag exhibits promising features for theranostics: half-life of 7.45 d, beta-emission with end-point energy 1036 keV, gamma-emission of 342 keV with 6.7% intensity. $^{111}$Ag can be produced in nuclear reactors via radiative neutron capture on enriched $^{110}$Pd targets. An alternative production route is via proton-induced fission of uranium carbide targets. The ISOLPHARM project plans to produce $^{111}$Ag with this reaction at the SPES Isotope Separation On-Line (ISOL) facility of INFN-LNL (Andrighetto et al., 2019).

Developing a TRT candidate based on $^{111}$Ag requires a long series of tests both at the preclinical and clinical phases. *In vitro* studies of radiopharmaceuticals require the ability to image the distribution of accumulated radionuclides in cells. Typically, this information is obtained from autoradiography images, in which the local distribution of radionuclides is recorded. The ISOLPHARM collaboration is developing a device able to perform autoradiography: the Detector Using Maps for Beta-rays Observations (DUMBO). This detector can provide images of medical beta-emitting radionuclides, such as $^{177}$Lu, $^{90}$Y, $^{131}$I. In particular, it is suitable for the beta energy spectrum of $^{111}$Ag (Arzenton, 2023; Donzella et al., 2025).

* Corresponding author at: Legnaro National Laboratories, National Institute for Nuclear Physics, INFN-LNL, Viale dell'Università 2, 35020 Legnaro, Italy.
*E-mail address:* davide.serafini@lnl.infn.it (D. Serafini).

https://doi.org/10.1016/j.apradiso.2026.112839
Received 4 May 2026; Received in revised form 25 June 2026; Accepted 27 July 2026
Available online 3 August 2026

### 1.2. State of the art of beta-imaging

Imaging of beta-emitting radionuclides has been performed using scintillator foils with a technique called RadioLuminescence Microscopy (RLM). In this case, the cell culture is positioned on top of a scintillator plate with 100 µm thickness. An inverted microscope collects the scintillation light produced by the $\beta$-rays generated in the radioactive decays on an EM-CCD. Using $^{18}$F positioned directly on top of the scintillator plate, this system is able to reach a FWHM of 5 µm (Pratx et al., 2012). Recently, a prototype employing budget-effective CMOS devices has been proposed with the name Lensless RadioMicroscope (LRM) (Klein et al., 2023). LRM can achieve a spatial resolution comparable with the one of the scintillator foil systems. Also with this device the cells have to be deposited directly on top of the CMOS to minimize the sample-detector distance. Consequently, the field of view (FOV) is limited to the sensor size. The cited LRM prototype employed a Raspberry Pi camera V2.1 equipped with a Sony IMX219 sensor; therefore its FOV is approximately $3.79 \times 2.69\,\mathrm{mm}^2 \approx 0.1\,\mathrm{cm}^2$ (Raspberry, 2026).

Another device commonly used for autoradiography is the Imaging Plate (IP). IPs feature FOV as large as $36 \times 43\,\mathrm{cm}^2$; however, they require an image processing step that cannot be performed during acquisition (Mori and Oikawa, 1997).

### 1.3. DUMBO beta-imaging device

RLM and LRM offer exceptional spatial resolution but require invasive or contact-based procedures, whereas IPs provide a large FOV at the cost of requiring a separate readout step. In this framework, the ISOLPHARM collaboration proposes the DUMBO imaging device for autoradiography, which avoids both invasive sample handling and offline data processing. Contamination is prevented by keeping the sample in a dedicated chambered coverslip. Consequently, the sample-detector distance is larger than 100 µm and the spatial resolution is lower than that of RLM and LRM. On the other hand, DUMBO features the ALice PIxel DEtectors (ALPIDE) chip, which provides a wide FOV of about 1.5 cm × 3 cm. While IPs also feature very large FOVs and good spatial resolution, they are limited to offline data analysis. Conversely, DUMBO is able to perform real-time imaging, enabling feedback during the experiments. Therefore, DUMBO is particularly suited for three-dimensional (3D) cell cultures, which have emerged as alternatives to better reproduce the *in vivo* tumor microenvironment (Abuwatfa et al., 2024). In fact, unlike 2D monolayer cultures typically investigated with microscopy-based autoradiography, 3D culture systems (e.g., spheroids or organoids) can span several millimeters and exhibit spatially heterogeneous radionuclide uptake across the entire structure (Haycock, 2011; Pekeč et al., 2023). In this work the first experiments aimed at the characterization of this device are presented.

The DUMBO device is not intended for microautoradiography at the single-cell or sub-cellular level, which typically requires micrometric spatial resolution and strict sample-detector proximity. Instead, its target application is the imaging of radionuclide distributions over extended areas, such as entire 2D and 3D cell cultures, where millimeter-to-submillimeter spatial resolution is sufficient to capture heterogeneous uptake patterns. In this framework, DUMBO should be considered as a complementary technique to high-resolution microscopy-based systems, prioritizing non-invasive operation, large FOV, and real-time capability over ultra-high spatial resolution.

## 2. Material and methods

### 2.1. ALPIDE chip

DUMBO incorporates several ALPIDE chips to detect beta particles emitted during the radioactive decay of radionuclides, such as $^{111}$Ag. The ALPIDE chips have been developed to be used in the inner tracking system of the ALICE experiment at CERN-LHC (Mager, 2016). Each chip has 512 × 1024 pixels realized with the Monolithic Active Pixel Sensor (MAPS) technology. Its high pixel density and low material budget make the ALPIDE a good candidate for medical applications where high spatial resolution is required (Varga-Kofarago, 2019; Colamaria et al., 2019). Each pixel contains a continuously active discriminating amplifier and a buffer capable of storing multiple events. Only pixels with an analog signal above a predefined threshold are processed, providing intrinsic zero suppression. The detected hits are stored locally and read out asynchronously toward the chip periphery, from where the data are transmitted off-chip in a First-In First-Out (FIFO) fashion.

The final design features 8 chips in a layout with 2 rows and 4 columns, for a total sensitive area equal to 3 cm × 12 cm. For the experiment described in Section 3.1, a smaller version with 2 chips and 3 cm × 3 cm sensitive area was used. The ALPIDE chips were operated without active cooling, as preliminary tests indicated that the thermal noise level was sufficiently low for the intended application. This is consistent with the low power consumption of the sensors, which allows stable operation at room temperature under our experimental conditions. In the future, an active cooling system could be implemented if tighter temperature control becomes necessary, for instance in scenarios requiring improved noise stability or operation under more demanding conditions.

### 2.2. DAQ

Prior to the DUMBO design, a desktop system featuring a single ALPIDE chip was developed to test an alternative DAQ solution (Bortolato, 2020). This prototype featured a Field Programmable Gate Array (FPGA) Digilent Arty A7 and an Arduino shield. The Python code written to control this hardware, after small modifications, could be used to control the DUMBO system too.

The DUMBO electronics consists of: a custom electronic *carrier* board; four *mezzanine* boards plugged in the carrier; two ALPIDE chips on each mezzanine; a *USB* board featuring a FT2232H Mini module and a small FPGA.

The carrier board has two banana plugs, used to collect the 5 V necessary to operate the ALPIDE chips from a power supply. In the experiment described in Section 3.1, the ALPIDE chips were powered by a RSPD 3303X-E bench power supply: output voltage from 0 to 32 V and output current up to 3.2 A. During an acquisition, each ALPIDE chip typically draws 90 mA. Each mezzanine corresponds to a channel in the carrier and in the USB board, connected via RJ45 sockets. The USB board is connected to a PC via a USB cable. A scheme showing the electrical connection is shown in Fig. 1.

The ALPIDE chips are controlled using the differential control ports DCTRL_P and DCTRL_N (ALICE ITS ALPIDE development team, 2017). The same ports are used also to read the signal, with a maximum speed of 40 Mbps. Using the dedicated ports, a reading speed of 1200 Mbps can be achieved theoretically. On the other hand, the design of electronics able to sustain this speed cannot be obtained easily. For the present DUMBO prototype, the reading speed provided by the differential control ports is sufficient. A Python code was developed to send the necessary commands to the chip and to read the data. The communication with the USB board is managed by the `pySerial` module, the code simply provides the string containing the message. The messages are used to manage the ALPIDE chip settings and to ask for the recorded data (ALICE ITS ALPIDE development team, 2017). The values set for the parameters are reported in Table 1. A single data query is basically a four-characters string. To retrieve more than one piece of data from the chips, a string constituted by multiple data queries is sent on the serial port. After a delay (30 ms) in which the chips accumulate the data, the PC reads on the serial port the expected number of data bytes updating the hits list. Each hit consists of the coordinates of the triggered pixel. This cyclic read-out continues until the interval time specified for the acquisition is up (Gambaro, 2025). Fig. 2 schematically represents the workflow described above.

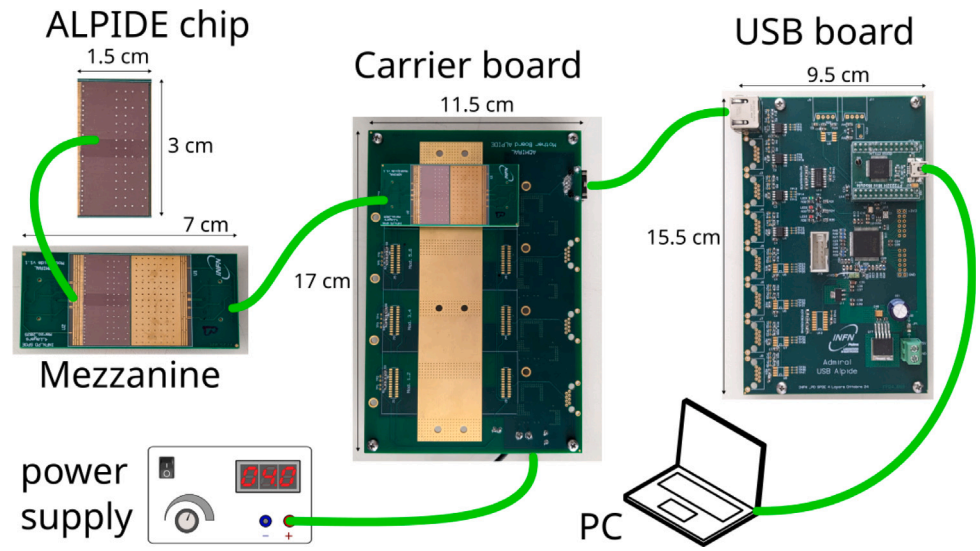


**Fig. 1.** Scheme of the electronics implemented in DUMBO. In this scheme, the single-ALPIDE configuration is shown: 1 of 2 ALPIDE chips in the mezzanine board and 1 of 4 mezzanine boards in the carrier board.

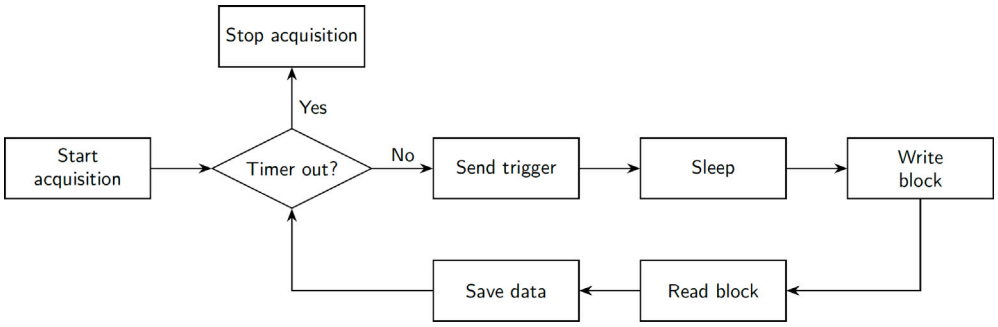


**Fig. 2.** Scheme representing the workflow of the acquisition system.

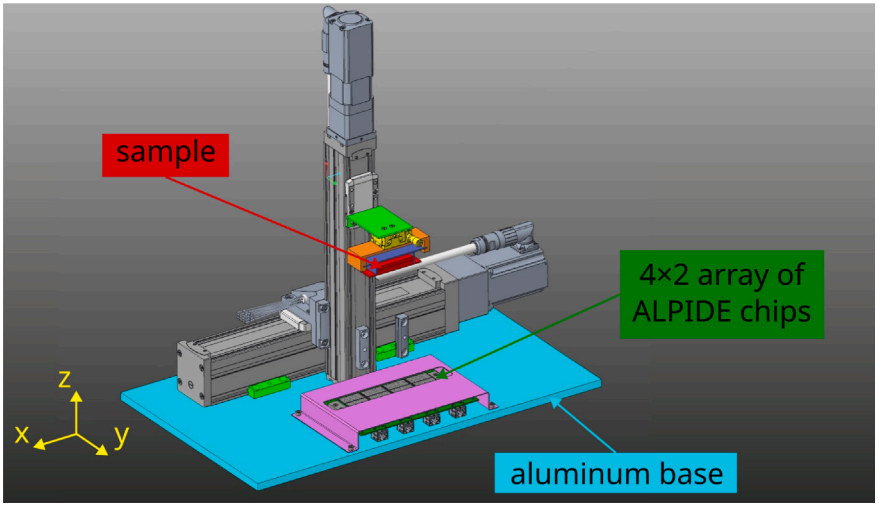


**Fig. 3.** 3D model of DUMBO. The two motors used to provide the movement along the two axes are visible. The set of ALPIDE chips is fixed on an aluminum base.

### 2.3. Mechanical layout

To optimize the sensitive area of the ALPIDE chips and the spatial resolution, a 3D movement between the sample and the ALPIDE chips is provided (see Fig. 3). In this setup, the sample can be moved along three directions while the ALPIDE chips are fixed. The movement mechanics was realized using two ball screw axes with repetition accuracy of 15 μm. Each axis is coupled to a stepper motor with 1.8° steps and 5% tolerance. The two motors can move automatically the sample in the x-z axes. To manually move the sample in the y axis, the last of the three axes, a single-axis translation stage is mounted. The stage has

**Table 1**
List of parameters and corresponding values chosen for the experiments. The description of the available parameters can be found in the ALPIDE manual (ALICE ITS ALPIDE development team, 2017).

| Address | Value | Description |
|---|---|---|
| 0 × 0001 | 0 × 020A | continue readout at 20 MHz, no clustering |
| 0 × 0004 | 0 × 0000 | disable busy monitoring |
| 0 × 0005 | 50 000 | strobe duration (≃ 1.25 ms) |
| 0 × 0006 | 5000 | strobe gap (≃ 125 µs) |
| 0 × 0010 | 0 × 0060 | disable Manchester encoding |
| 0 × 0602 | 0 × 0093 | set reset voltage of the charge collecting node |
| 0 × 060E | 53 | ITHR pixel charge threshold (about 0.5 nA) |

a travel range of 6.5 mm actuated through a 10 µm graduated head. The motors are powered via the CMMT-ST-C8-1C-MP-S0 module. This module can be connected to a PC via Ethernet cable without the need for a PLC (Coppelli, 2025).

A commercial software is available to move the employed motors: the *Festo Automation Suite v2.9.1.1*. Using the software GUI multiple routines of actions can be defined and used in different types of acquisitions. The user can launch a single acquisition with default positioning. Or multiple images with different sample positions can be acquired and subsequently merged into one single picture. A Python module, named `festo-edcon`, can be used to manage the motors within a Python script.

### 2.4. Geant4 simulation

The Geant4 toolkit v11.3.0 was used to build a Monte Carlo simulation framework (Agostinelli et al., 2003; Allison et al., 2006, 2016). The simulation can be tuned according to the characteristics of the sample, the updated version is available online (Pavanello, 2023; Busatto, 2025). Each ALPIDE chip is realized as a 512 × 1024 matrix of silicon boxes with dimensions 28 µm × 28 µm × 50 µm. On top of each chip there is a 11 µm thick layer made of silicon oxide $SiO_2$. Below each chip there is a 14 µm layer made of silicon that serves as a support. The sensitive elements are the single silicon pixels. The output of the simulation is a ROOT file containing both histograms and tuples. The histograms contain pre-analyzed data such as the hitmap and the energy spectrum. The tuples enable the study of correlations between hits belonging to the same event. This information is required to reconstruct, in the simulated data, the clusters produced by single electron tracks, which are identified by the real DAQ system and processed with case-specific operations, as described in Section 2.2. The physics lists adopted are: `G4EmStandardPhysics`, `G4DecayPhysics` and `G4RadioactiveDecayPhysics`. Electron neutrinos and antineutrinos are killed at the generation. The default Geant4 production range cut was used. The primary particles are radionuclides, in particular $^{111}$Ag.

The simulation framework was validated using the data from the first experimental characterization of DUMBO, described in the next section. Specifically, the results obtained with the GelMA (Gelatin Methacrylic Anhydride) phantom were used. For the study of 3D cell cultures, mixtures containing 95% water and 5% GelMA are commonly used as a base for 3D bioprinting. Therefore, in both the experiment and the simulation presented here, a hydrogel box made of GelMA was used.

### 2.5. Experimental protocol

For the experiment described in this work, $^{111}$Ag produced in the LENA laboratory of Pavia was used. The radionuclide was delivered in a water solution that was inserted in three different types of containers: in plastic vials, in plastic phantoms and in GelMA phantoms (Gaglio et al., 2024). The plastic vials had a diameter of 6 mm and 12 mm. The liquid GelMA was inserted in a chambered coverslip with a polymeric bottom 180 µm thick. The GelMA was cured using a UV lamp with 405 nm emission and 6 W power. The plastic phantoms were made in Polyoxymethylene (POM), and their dimensions were chosen to be as close as possible to those of the GelMA phantoms. Figs. 5(a) and 6(a) show the schematic diagrams of the plastic and GelMA phantoms respectively. The activity of the $^{111}$Ag samples was measured using a germanium gamma-ray detector. Due to the heterogeneous sample shapes, a 10 % uncertainty is associated to the activity estimations present in this work.

## 3. Results

### 3.1. Images with vials and plastic phantoms

An experimental session was carried out to evaluate the performance of this device with the radionuclide of interest: $^{111}$Ag. The radionuclide was produced in the LENA lab of Pavia and was available in water solution. Several images were collected using samples with different amount of activity and different shapes. The vial with 12 mm diameter containing the stock solution, 7.92 MBq of $^{111}$Ag in 1 mL of water, was imaged in the first test. The detector spatial resolution is sufficient to recognize the circular shape of the sample (Fig. 4(a)). The two subplots represent the sensitive areas of the two ALPIDE chips. Also for the small vial containing 10 µL of the stock solution (79 kBq of $^{111}$Ag), the vial circular shape can be recognized (Fig. 4(b)). In both images, a darker corona is visible around the central area. This effect can be explained by the fact that the base of the vials is thicker at the edges. Outside this dark corona, counts are still visible; this can be explained by the fact that the air surrounding the vial attenuates electrons less effectively than the vial material.

Another set of acquisitions was performed using plastic (POM) phantoms. Multiple phantoms were prepared for this experiment but only one of them will be considered here for the sake of conciseness. The phantom is a 25 × 65 × 7 mm$^3$ POM brick where three pockets host the radioactive solution (Fig. 5(a)). The pockets are 15 mm long and have different widths: 1 mm, 2 mm and 3 mm. A circular notch with 3 mm diameter facilitates the insertion of the solution via a micropipette. The FOV of DUMBO is able to cover only two pockets per time. The pockets imaged in this acquisition are indicated with a dashed line on the technical drawing. The corresponding image is shown in Fig. 5(b). As expected, the pocket with larger width has a signal wider than the smaller pocket. A profile along the $x$-axis, Fig. 5(c), shows a FWHM of about 3.1 mm and 2.6 mm for the 3 mm and 2 mm slots respectively.

### 3.2. Images with GelMA phantoms

Following the characterization with plastic phantoms, which provide better control over the source geometry, GelMA phantoms were employed to test an acquisition with $^{111}$Ag embedded in the same medium used to host the 3D cell cultures. $^{111}$Ag is inserted in three wells inside the phantom as schematically represented in Fig. 6(a). The sample was then imaged by DUMBO and the resulting image can be seen in Fig. 6(c). Three $^{111}$Ag spots were created depositing a small quantity of radioactive GelMA, prepared using the $^{111}$Ag solution, and curing them with UV light. The expected result was calculated through a Geant4 simulation and featured three circular clusters, as shown in Fig. 6(d). Even if the GelMA phantoms had wells to host the drops of radioactive solution, there was some leakage and contamination in the surrounding area, visible also in the picture in Fig. 6(b). In fact, a signal halo can be recognized below the first spot at the left of the acquired image in Fig. 6(c). The detected $^{111}$Ag signal seems contained within the prepared wells, suggesting that no relevant diffusion took place in the time interval between the sample preparation and the measurement, which was about 15–20 min.

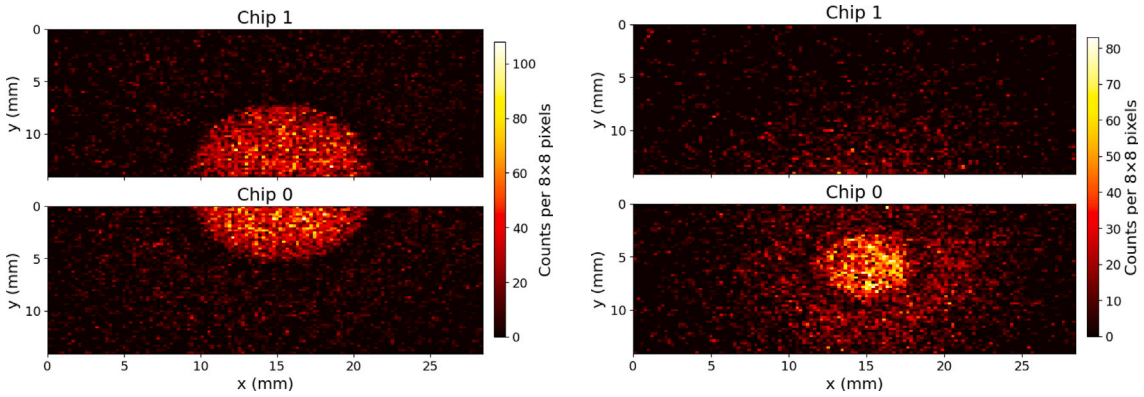


(a) 12 mm diameter vial (b) 6 mm diameter vial

**Fig. 4.** Images of vials containing $^{111}$Ag solution. The acquisition time is 120 s for each image. The physical separation between the two chips is about 0.5 mm and is not to scale in the reproduced images.

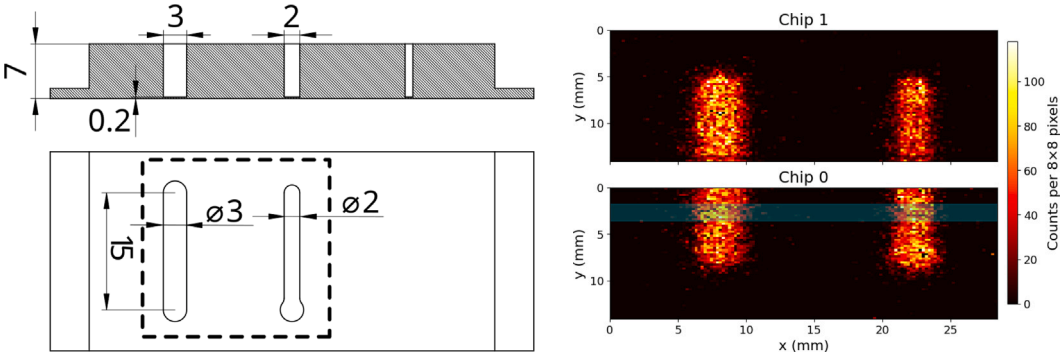


(a) Technical drawing of the phantom, distance values in millimeters. The rectangle with the dashed outline indicates the area experimentally measured by the device and shown in Fig. 5(b).

(b) Hitmap of the phantom. Binning 8 × 8 is used. The acquisition time is 120 s. The cyan band indicates the bins used to plot the profile shown in Fig. 5(c).

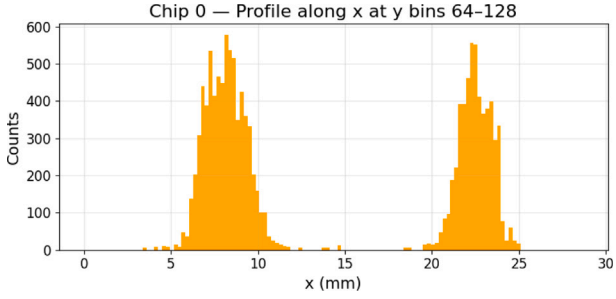


(c) Profile along the x-axis

**Fig. 5.** Plastic phantom acquisition with $^{111}$Ag solution.

### 3.3. Simulated spatial resolution

Using the Geant4 toolkit, point-like sources of $^{111}$Ag were simulated at different distances from the detector surfaces. The profiles obtained selecting only the bins with $y = 0$ mm are shown in Fig. 7. For both profiles, $10^6$ radioactive nuclei were generated. Each profile is fitted with a Gaussian function using the `SciPy` library. The obtained FWHMs are 0.311(5) mm and 1.26(2) mm, for the sources at 100 µm and 500 µm distance respectively.

## 4. Discussion

The Monte Carlo simulations show that the spatial resolution of the Point Spread Function (PSF) worsens as the source-to-detector distance increases. This effect is evident for DUMBO and, more generally, also applies to other types of $\beta$-imaging systems (Klein et al., 2023). Therefore, the preparation of the sample must be done carefully to minimize the source-to-detector distance. The sources used during the experiments presented in this work could not be positioned as close to the detector as required for sub-millimetric imaging. Moreover, the

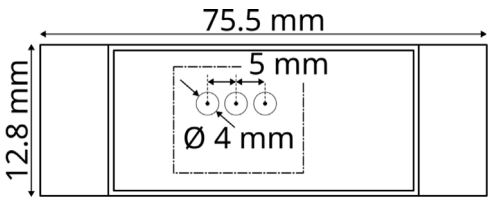


(a) Scheme of the GelMA phantom. The rectangle with the dashed outline indicates the area experimentally measured by the device.

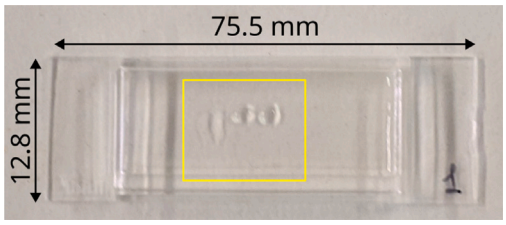


(b) Picture of the GelMA phantom. The rectangle with the yellow outline indicates the area experimentally measured by the device and shown in Fig. 6(c). Inside this area, there are three $^{111}$Ag spots.

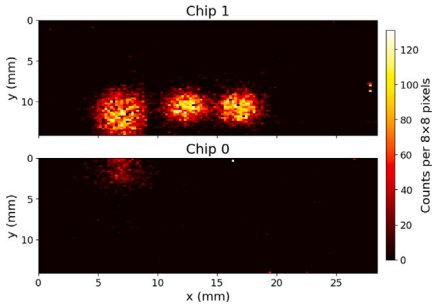


(c) Hitmap of the GelMA phantom. The acquisition time is 120 s. The three disks correspond to the three $^{111}$Ag spots visible in the yellow square of Fig. 6(b).

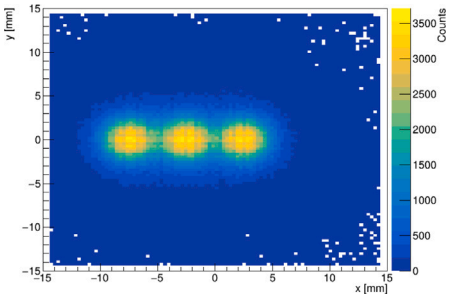


(d) Geant4 simulation of the GelMA phantom. The three $^{111}$Ag spots have 2 mm diameter and their centers are separated by a 5 mm distance. Adapted from Busatto (2025).

**Fig. 6.** GelMA phantom acquisition with $^{111}$Ag solution.

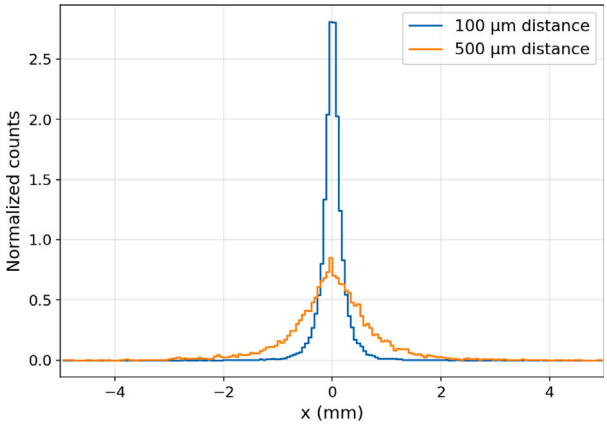


**Fig. 7.** Profiles of simulated images of $^{111}$Ag point-like sources at different distances from the detector surface. Each profile is obtained considering only the bins with $y = 0$ mm.

GelMA material, which can be used as a sample scaffold, could not be used to realize geometries with details smaller than 1 mm.

At the same time, the simulations indicate that DUMBO should be able to reach a sub-millimetric spatial resolution. In particular, a source-to-detector distance of 100 µm determines a FWHM of about 0.3 mm with a $^{111}$Ag source. Therefore, the main limitation in practical applications is the achievable source-to-detector distance.

The present measurements demonstrate the capability of DUMBO to detect and image $^{111}$Ag samples with activities of the order of 100 kBq. The images presented in this work were all acquired with an acquisition time of 120 s. Nonetheless, the acquisition time can be adjusted according to the activity of the sample. However, a systematic study of the linearity between sample activity and detected counts was not performed. Therefore, the current data should not be interpreted as a quantitative calibration of the detector response.

## 5. Conclusions

In this work, the development and characterization of an autoradiography device named DUMBO are presented. The device enables non-invasive imaging of both 2D and 3D cell cultures. Its main advantages are a wide FOV of 3 cm × 3 cm, real-time image reconstruction, and ease of use. On the other hand, the spatial resolution is lower than that of typical radioluminescence microscopy. Monte Carlo simulations indicate that, for a source–detector distance of 100 µm, the intrinsic system resolution reaches a FWHM of about 0.3 mm. DUMBO was tested in an experiment using $^{111}$Ag produced at the LENA laboratory in Pavia, demonstrating its capability to capture $^{111}$Ag distributions. Furthermore, GelMA phantoms were fabricated and imaged to assess the applicability of DUMBO for 3D samples.

## CRediT authorship contribution statement

**Davide Serafini:** Writing – review & editing, Writing – original draft, Visualization, Validation, Software, Methodology, Investigation, Formal analysis, Conceptualization. **Jessica Carolina Delgado Alvarez:** Writing – review & editing, Visualization, Software, Methodology, Investigation, Conceptualization. **Aurora Leso:** Writing – review & editing, Visualization, Investigation, Conceptualization. **Alberto Arzenton:** Writing – review & editing, Conceptualization. **Devid Maniglio:** Writing – review & editing, Resources, Conceptualization. **Stefano Corradetti:** Writing – review & editing, Resources, Conceptualization. **Emilio Mariotti:** Writing – review & editing, Supervision, Resources, Conceptualization. **Marcello Lunardon:** Writing – review & editing, Writing – original draft, Visualization, Validation, Supervision, Software, Resources, Project administration, Methodology, Conceptualization. **Piero Giubilato:** Writing – review & editing, Supervision, Resources, Conceptualization. **Alberto Andrighetto:** Writing – review & editing, Supervision, Funding acquisition, Conceptualization.

## Declaration of competing interest

The authors declare that they have no known competing financial interests or personal relationships that could have appeared to influence the work reported in this paper.

## Acknowledgments

This research is part of the ADMIRAL experiment, funded by CSN5 of INFN. The $^{111}$Ag radionuclide solution and the laboratory facilities used for the experiment were provided by LENA in Pavia. The authors would like to thank the INFN-BO workshop staff, the UNIPD-DFA staff, and the UNIPV-DSCCDP staff for their technical support. The authors also gratefully acknowledge the bachelor's and master's students who contributed to this activity through their theses: S. Busatto, T. Coppelli, E. C. Gambaro, and V. Pavanello. During the preparation of this work, the authors used Microsoft Copilot to improve language and readability. After using this tool, the authors reviewed and edited the content as needed and take full responsibility for the content of the publication.

## Data availability

Data will be made available on request.

## References

Abuwatfa, W.H., Pitt, W.G., Husseini, G.A., 2024. Scaffold-based 3d cell culture models in cancer research. J. Biomed. Sci. 31, http://dx.doi.org/10.1186/s12929-024-00994-y.

Agostinelli, S., Allison, J., Amako, K., et al., 2003. Geant4—a simulation toolkit. Nucl. Instrum. Methods Phys. Res. A 506, 250–303. http://dx.doi.org/10.1016/s0168-9002(03)01368-8.

ALICE ITS ALPIDE development team, 2017. ALPIDE operations manual. Technical Report, CERN, URL: https://edms.cern.ch/document/1773020/1.

Allison, J., Amako, K., Apostolakis, J., et al., 2006. Geant4 developments and applications. IEEE Trans. Nucl. Sci. 53, 270–278. http://dx.doi.org/10.1109/tns.2006.869826.

Allison, J., Amako, K., Apostolakis, J., et al., 2016. Recent developments in geant4. Nucl. Instrum. Methods Phys. Res. A 835, 186–225. http://dx.doi.org/10.1016/j.nima.2016.06.125.

Andrighetto, A., Tosato, M., Ballan, M., Corradetti, S., Borgna, F., Di Marco, V., Marzaro, G., Realdon, N., 2019. The ISOLPHARM project: ISOL-based production of radionuclides for medical applications. J Radioanal Nucl Chem 322, 73–77. http://dx.doi.org/10.1007/s10967-019-06698-0.

Arzenton, A., 2023. Radiobiological model for $\beta$-emitter radiopharmaceutical therapy in dynamic cell cultures in the framework of the ISOLPHARM project. Nuovo Cimento C 46, 1–10. http://dx.doi.org/10.1393/ncc/i2023-23072-3.

Bortolato, G., 2020. Sviluppo del firmware per il controllo del detector ALPIDE ed implementazione su FPGA. (Bachelor thesis). Università degli Studi di Padova, URL: https://hdl.handle.net/20.500.12608/22415.

Busatto, S., 2025. Simulazione dei campioni di idrogel biologico caricati con ag-111 e prime caratterizzazioni sperimentali con il beta detector DUMBO (Bachelor thesis). Università degli Studi di Padova, URL: https://hdl.handle.net/20.500.12608/92748.

Colamaria, F., Trombetta, G., Bruno, G.E., De Robertis, G., Manzari, V., Mazzone, A., Pastore, C., 2019. Study of the photon rejection of the alpide pixel detector for medical applications. In: 2019 IEEE 8th Int Workshop Adv Sens Interfaces. IWASI, IEEE, pp. 1–6. http://dx.doi.org/10.1109/iwasi.2019.8791306.

Coppelli, T., 2025. Studio della meccanica di precisione per il posizionamento dei campioni biologici sul rivelatore per radiazione beta DUMBO dell'esperimento ADMIRAL (Bachelor thesis). Università degli Studi di Padova, URL: https://hdl.handle.net/20.500.12608/92751.

Donzella, A., Leso, A., Arzenton, A., Bonomi, G., Bortolussi, S., Chen, D., Corradetti, S., Lunardon, M., Mariotti, E., Reniero, E., Serafini, D., Valli, G., Zangrando, L., Zenoni, A., Andrighetto, A., 2025. Monte carlo dosimetry of silver-111 in simplified cell geometries in the framework of the isolpharm project. Appl. Radiat. Isot. 225, 111979. http://dx.doi.org/10.1016/j.apradiso.2025.111979, URL: https://www.sciencedirect.com/science/article/pii/S0969804325003240.

Gaglio, C.G., Baruffaldi, D., Pirri, C.F., Napione, L., Frascella, F., 2024. Gelma synthesis and sources comparison for 3d multimaterial bioprinting. Front. Bioeng Biotechnol Volume 12 - 2024, http://dx.doi.org/10.3389/fbioe.2024.1383010, URL: https://www.frontiersin.org/journals/bioengineering-and-biotechnology/articles/10.3389/fbioe.2024.1383010.

Gambaro, E.C., 2025. Sviluppo del software di comunicazione e prime misure di caratterizzazione del rivelatore per beta-imaging DUMBO nel contesto del progetto ISOLPHARM (Bachelor thesis). Università degli Studi di Padova, URL: https://hdl.handle.net/20.500.12608/92750.

Haycock, J.W., 2011. 3D Cell Culture: A Review of Current Approaches and Techniques. Humana Press, Totowa, NJ, pp. 1–15. http://dx.doi.org/10.1007/978-1-60761-984-0_1, chapter 1.

Klein, J.S., Kim, T.J., Pratx, G., 2023. Development of a lensless radiomicroscope for cellular-resolution radionuclide imaging. J. Nucl. Med. 64, 479–484. http://dx.doi.org/10.2967/jnumed.122.264021, URL: https://jnm.snmjournals.org/content/64/3/479.

Mager, M., 2016. Alpide, the monolithic active pixel sensor for the alice its upgrade. Nucl. Instrum. Methods Phys. Res. A 824, 434–438. http://dx.doi.org/10.1016/j.nima.2015.09.057, URL: https://www.sciencedirect.com/science/article/pii/S0168900215011122.

Mori, N., Oikawa, T., 1997. The imaging plate and its applications. Advances in Imaging and Electron Physics. Elsevier, pp. 241–290. http://dx.doi.org/10.1016/s1076-5670(08)70243-x.

Pavanello, V., 2023. Performance study of a novel 2D imaging beta detector for medical applications (Master's thesis). Università degli Studi di Padova, URL: https://hdl.handle.net/20.500.12608/51901.

Pekeč, T., Venkatachalapathy, S., Shim, A.R., Paysan, D., Grzmil, M., Schibli, R., Béhé, M., Shivashankar, G.V., 2023. Detecting radio- and chemoresistant cells in 3d cancer co-cultures using chromatin biomarkers. Sci. Rep. 13, http://dx.doi.org/10.1038/s41598-023-47287-2.

Pratx, G., Chen, K., Sun, C., Martin, L., Carpenter, C.M., Olcott, P.D., Xing, L., 2012. Radioluminescence microscopy: Measuring the heterogeneous uptake of radiotracers in single living cells. PLoS One 7, 1–9. http://dx.doi.org/10.1371/journal.pone.0046285.

Raspberry, 2026. URL: https://www.raspberrypi.com/documentation/accessories/camera.html#hardware-specification.

Sgouros, G., Bodei, L., McDevitt, M.R., Nedrow, J.R., 2020. Radiopharmaceutical therapy in cancer: clinical advances and challenges. Nat Rev Drug Discov 19, 589–608. http://dx.doi.org/10.1038/s41573-020-0073-9.

Varga-Kofarago, M., 2019. Medical applications of the alpide detector. Universe 5, http://dx.doi.org/10.3390/universe5050128, URL: https://www.mdpi.com/2218-1997/5/5/128.